https://doi.org/10.5194/egusphere-2026-1010
Preprint. Discussion started: 10 March 2026

Title:
Detection of agricultural flash droughts using impact-informed thresholds

Ingrid Ubeda-Trujillo[1, 2, 3], Micha Werner[1], Claudia Bertini[1], Miriam Coenders-Gerrits[2], and Graham Jewitt[1,2]
[1]IHE Delft Institute for Water Education, P.O. Box 3015, 2601 DA Delft, the Netherlands
[2]Delft University of Technology, Department Water Management. Section, P.O. Box 5048, 2600 GA Delft, the Netherlands
[3]Universidad Nacional Autónoma de Nicaragua, UNAN-Managua. Rigoberto López Pérez roundabout, 150m east.
Correspondence to: i.ubedatrujillo@tudelft.nl

Abstract

A rapid and sustained evaporative stress causes soils to lose moisture within days to weeks during sensitive crop phases. This rapid soil depletion can severely affect agricultural systems and manifest as events commonly referred to as agricultural flash droughts (AFDs). AFDs are often detected using literature-based thresholds that assume uniformity across time and space. This may, however, poorly represent the occurrence and impacts of AFDs in local contexts and limit usefulness to decision-makers who require context-specific information. This study aims to overcomes these limitations by introducing an impact-informed calibration of the Standardized Evaporative Stress Ratio (SESR) by linking SESR thresholds to observed crop losses. Thresholds are derived temporally across crop management periods and spatially across soil textures. The proposed calibration approach is tested in Nicaragua's Dry Corridor of Central America, where rainfed agriculture predominates. Results suggest that although SESR exhibits coherent evaporative stress signals during years with drought-induced crop losses, literature-based thresholds showed limited skill in translating these signals into agriculturally relevant flash drought detection across different crop management periods and soil textures. Threshold performance varies across crop management periods and soil textures. Reliable thresholds could not be detected in sandy soils, whereas clay-rich soils exhibited stable and skilful thresholds. In loamy–silty soils, skilful thresholds were mainly observed during March and the pre-sowing period, with limited skill thereafter. Validation results also showed that calibrated thresholds, within the crop periods-soil combinations identified as skilful, successfully detected flash drought events associated with crop losses more frequently than those reported in the literature. Together, these findings indicate that monitoring AFD using impact-informed thresholds has an operational value for drought management and can support better decision-making.

Keywords: Evaporative stress; Impact-informed thresholds; Crop management periods; Soil Textures, Dry Corridor; Drought monitoring

1. Introduction

Drought is one of the major climate-related hazards affecting crop yields, particularly in dryland regions dominated by rainfed systems (Kibler et al., 2023; Verbist et al., 2018). This hazard thus undermines progress towards Sustainable Development Goals 1, 6 and 13. Drought arises when a prolonged lack of precipitation leads to low water availability in the soil, rivers, and reservoirs (Svoboda et al., 2002; Yuan et al., 2019). When these conditions are further intensified by high temperatures and evaporative stress that increase rapidly and persist over days to weeks, flash drought can develop (Basara et al., 2019; Noguera et al., 2022). Under these conditions, soils lose water faster than it is replenished, causing abrupt

https://doi.org/10.5194/egusphere-2026-1010
Preprint. Discussion started: 10 March 2026

soil moisture decline and severely affecting agricultural systems (Yuan et al., 2019). When such rapid depletion affects the sensitive crop growth stages in rainfed systems (Verbist et al., 2018), the resulting conditions are commonly referred to as agricultural flash droughts (AFDs) (Lovino et al., 2024). These events often evolve over only a few weeks, leaving limited time for farmers and institutions to adjust planting decisions, resource allocation, or short-term water management (Yuan et al., 2023). Because of the rapid onset and severe impacts on rainfed agriculture, AFDs are a critical climate-related risk that needs to be explicitly considered in early warning systems, risk management, and drought monitoring in dryland regions.

A widely used approach for flash drought detection relies on the Standardized Evaporative Stress Ratio (SESR), derived from the ratio of actual and potential evaporation (Edris et al., 2023; Otkin et al., 2022). In most applications, flash droughts are detected based on SESR and literature-based fixed percentile thresholds, implicitly assuming that a given percentile represents a comparable level of stress across regions and seasons. Yet percentiles are purely relative measures of rarity rather than of absolute stress, so a fixed percentile does not necessarily imply the same level of plant and soil-water stress everywhere (Hobbins and Huntington, 2016; Otkin et al., 2022). This assumption fails particularly in drylands with rainfed systems, because high evaporative demand and chronically low soil moisture make evaporative stress part of the normal background (Hobbins and Huntington, 2016; Kibler et al., 2023). In such settings, a fixed SESR percentile threshold does not consistently distinguish anomalous evaporative stress from background conditions across soil textures, and may not correspond to the same SESR levels at which agricultural impacts occur (Suliman et al., 2024; Yu et al., 2023). These issues highlight a broader methodological limitation of current SESR-based flash drought detection frameworks when applied across diverse climate and soil conditions.

Moreover, thresholds used in the literature are usually defined independently of the crop calendar, even though short dry spells during sensitive growth stages can cause damage (Verbist et al., 2018), while a similar stress outside these windows has limited impact (Bucheli et al., 2021; Teleubay et al., 2025). This creates a gap between when SESR anomalies are detected and when impacts occur in the local context. Others indicator such as the Vegetation Health Index (VHI) provides more direct evidence of agricultural stress on the ground, but it is reactive, signalling stress only after it has occurred (Li et al., 2023; Rojas, 2020). In contrast, SESR responds earlier to anomalies in the surface energy and water balance (Anderson et al., 2016; Hobbins and Huntington, 2016), offering a timely physically based signal of evaporative stress that has the potential to support operational use (Buitink et al., 2021; Leasor et al., 2020; Li et al., 2023; Teleubay et al., 2025) when appropriately calibrated (McEwen et al., 2021; Shyrokaya et al., 2024). This suggests that SESR could support improved detection and monitoring of agricultural relevant flash drought conditions if thresholds were calibrated to local agricultural conditions and impact evidence. However, there is still no widely applied approach to systematically calibrating SESR thresholds across both crop management periods and soil textures, particularly in dryland, rainfed systems, which limits the operational relevance of SESR for agricultural flash drought monitoring and management.

In many dryland regions, these limitations are particularly critical for smallholder rainfed systems, where flash droughts can quickly translate into crop failure, food insecurity, and income loss (Solh and van Ginkel, 2014) as has occurred in the Central American Dry Corridor of Nicaragua, where recurrent drought episodes have been associated with declining crop yields and heightened vulnerability among smallholder farmers. Strengthening agricultural flash

https://doi.org/10.5194/egusphere-2026-1010
Preprint. Discussion started: 10 March 2026

drought detection requires context-specific information that is essential for drought monitoring and management. This study addresses these limitations by calibrating SESR thresholds temporally across crop management periods and spatially across soil textures, using a benchmark of agricultural impacts. To do so, this physically based but standardised indicator was linked to locally observed drought-induced crop losses. The proposed approach aims to enhance the agricultural relevance of SESR-based flash drought detection for farmers and decision-makers in dryland, rainfed systems. Three main objectives were addressed: (i) to evaluate the potential agricultural relevance of the Standardized Evaporative Stress Ratio (SESR) for detecting anomalous evaporative stress during years with drought-induced crop losses, (ii) to calibrate and evaluate SESR thresholds across crop management periods and soil textures, and (iii) to validate literature-based and calibrated thresholds against locally independent agricultural benchmarks. In a wider context, the impact-based calibration approach which was tested in the Dry Corridor of Nicaragua offers a basis that could be adapted and tested in other dryland and rainfed regions and can support the integration of local informed and impact-based agricultural flash drought monitoring into drought management.

2. Data and methods

2.1 Overview of the study area: climate, agricultural, and edaphic context

To develop and test the calibration process, this study focuses on the Nicaragua Dry Corridor, specifically in the northern portion of the Rio San Juan basin. This basin comprises eight hydrological catchments and includes major rivers such as the Sinecapa and Pacora (INETER et al., 2014). The basin spans diverse landscapes: The northern part overlaps with protected areas including Yalí, Miraflor-Moropotente and Tizey-Estanzuela. The middle part includes Lake Managua, several crater lagoons and additional protected areas, while the southernmost part comprises the Tisma wetland, a Ramsar site. In total, the basin encompasses 31 municipalities and approximately 640 settlements. At a broader scale, the study area forms part of the Central America Dry Corridor, which includes the countries of Guatemala, El Salvador, Honduras, and Costa Rica, bounded by the Caribbean region to the east and the Pacific Ocean to the west.

Figure 1a-b shows that rainfed agriculture coverS approximately 40% of the study area (Teluguntla et al., 2023; Ubeda Trujillo and Rocha, 2020) with subsistence and commercial farming based on the main staples: beans and maize (van der Zee Arias et al., 2012). The main cropping cycle extends from May to August (Figure 1d), lasting about four months and including pre-sowing, sowing, growing (vegetative and flowering stages), and harvesting periods (Figure 1e). This cropping cycle coincides with the rainy season (Figure 1c). The average annual precipitation is about 800 mm/year, and mean temperatures are above 25°C for the whole year (van der Zee Arias et al., 2012). A notable climatological feature is the Canícula, a 10–20-day mid-summer dry spell, commonly occurring from mid-July to August linked to the El Niño-Southern Oscillation (Rojas et al., 2020). The Canícula temporally interrupts the rainy season and tends to intensify during El Niño years (Verbist et al., 2018). Atmospheric evaporative demand varies across climatic seasons and regions within the study area. Based on MOD16A2, during the dry season, in the east-central and south-central parts of the Pacific plains (46-80 m.a.s.l.), potential evaporation (PET) reaches 8.5–9.3 mm day^{-1} when aggregated over 10-day periods. In contrast, in the north-eastern and western parts of the mountainous areas (682–1004 m.a.s.l.), PET ranges from 7.5–8.3 mm day^{-1} (Salinas Marcenaro et al., 2023), reflecting elevated atmospheric evaporative demand before the onset of rains. PET decreases in both regions during the rainy season, with values of 4.5–6.0 mm day^{-1} in the Pacific plains and 3.5–4.5 mm day^{-1} in the mountainous ranges (Salinas Marcenaro et al., 2023). Overall, the Pacific shows the highest

https://doi.org/10.5194/egusphere-2026-1010
Preprint. Discussion started: 10 March 2026

evaporative demand through the year, while the northern mountain region exhibits the lowest PET, following a common annual pattern governed by the transition from the rainy to the dry season. The study area is characterised by six soil textures (DGOT, 2024): (1) coarser sandy, (2) moderately coarse sandy, (3) loamy and silty, (4) moderately fine clay-loam, (5) fine clayey, and (6) very fine expansive clayey soils (see Figure S1).

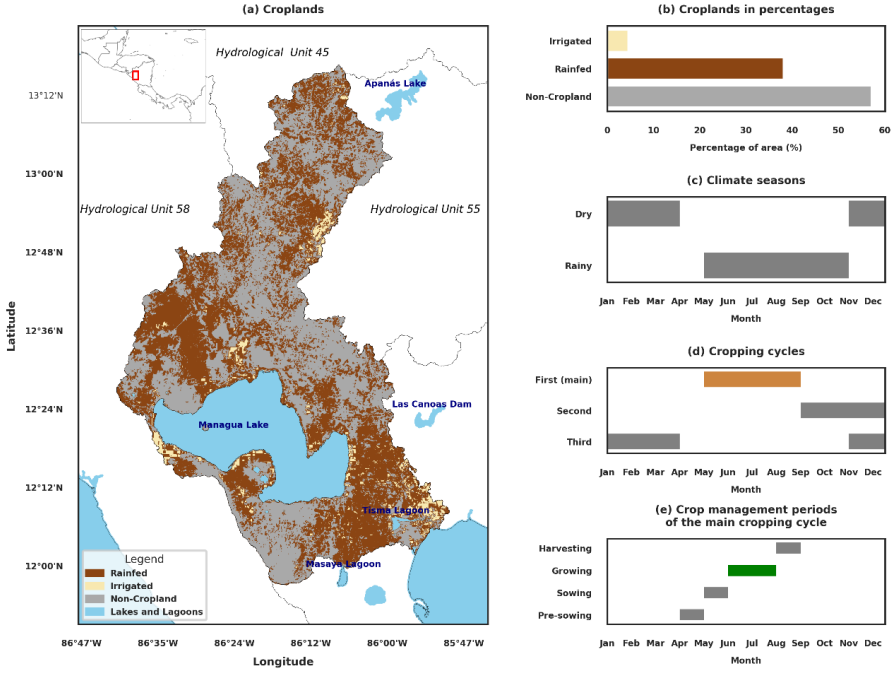

Figure 1. Overview of the northern part of the Rio San Juan basin. (a) croplands, (b) cropland in percentage, (c) climate seasons, (d) cropping cycles, and (e) crop management periods of the main cycle.

2.2 Data and preprocessing

Three main sources of data were used in this study: (1) MODIS MYD16A3GF (Steve et al., 2021), (2) Vegetation Health Index (FAO, 2014), and (3) qualitative information such as newspapers and reports. Qualitative information was compiled from the two oldest national newspapers in Nicaragua and from reports produced by GIEWS (Global Information and Early Warning System on Food and Agriculture; https://www.fao.org/giews/reports/giews-updates/en/), FEWS NET (Famine Early Warning Systems Network; https://fews.net/), and EM-DAT (The International Disaster Database; https://www.emdat.be/).

The MODIS dataset provides 8-day composites at 500 m spatial resolution from 2001 to 2024. From this dataset, actual evaporation (ET) and potential evaporation (PET) inputs were used to derive the Standardized Evaporative Stress Ratio (SESR) and the standardized changes in SESR following the approach of Christian et al. (2019). Preprocessing included (i) computing the Evaporative Stress Ratio as ET/PET; (ii) calculating long-term mean and standard deviation at each time step and grid point; and (iii) standardizing ESR into Standardized Evaporative Stress Ratio (SESR) using a z-score transformation:

https://doi.org/10.5194/egusphere-2026-1010
Preprint. Discussion started: 10 March 2026

$$SESR_{ijp} = (ESR_{ijp} - \overline{ESR}_{ijp}) / \sigma ESR_{ijp} \quad (1)$$

Where $SESR_{ijp}$ is the z-score of ESR at specific grid point (ij) and time step p. ESR_{ijp} is the evaporative stress ratio; and σESR_{ijp} is the corresponding standard deviation across all years. (iv) computing temporal changes in SESR (ΔSESR-z):

$$(\Delta SESR_{ijp})_z = (\Delta SESR_{ijp} - \overline{\Delta SESR}_{ijp}) / \sigma \Delta SESR_{ijp} \quad (2)$$

Where $\Delta SESR_{ijp}$ is the change of SESR at specific grid point (ij) and time step p. $\overline{\Delta SESR}_{ijp}$ and $\sigma \Delta SESR_{ijp}$ are long-term mean and standardized deviation, respectively.

The Vegetation Health Index (VHI) dataset has a 1 km spatial resolution and is available from 1984 to 2024. Seven preprocessing steps are applied to ensure quality and temporal/spatial compatibility with SESR. This includes: (i) a range filtering that removes values outside the valid domain 0-1 (Kogan, 1995), (ii) an empirical saturation adjustment that smooths persistent maximum values (VHI =1) to reduce saturation artifacts (Gu et al., 2013), (iii) a conversion of decadal labels to ISO 8601 dates to ensure standardized time representation for further alignment; (iv) a resampling to 8-day intervals that aligns VHI to the temporal resolution of MODIS-based SESR products, (v) a linear temporal interpolation to 8-day resolution to fill temporal gaps and enable regular time-series analysis (Soltani et al., 2004), (vi) a spatial filling of voids through nearest-neighbour interpolation within valid data areas (Teoh et al., 2008), and (vii) a comparison of the original data with the final 8-day resampled version at various spatial points to evaluate the reliability of the harmonization process from the temporally interpolated dataset.

2.3 Spatial and temporal calibration approach

The spatial and temporal calibration of SESR approach proposed here is summarized in six parts. The spatial and temporal sampling design is presented in Sect. 2.3.1. The baseline benchmarks of drought-induced crop losses are described in Sect. 2.3.2. The detection of agricultural flash droughts is detailed in Section 2.3.3. In Sect. 2.3.4, a diagnostic assessment of the Standardized Evaporative Stress Ratio (SESR) is conducted prior to calibration. The calibration of SESR thresholds, including performance metrics and uncertainty analysis, is introduced in Sect. 2.3.5. Finally, the validation strategy for literature-based and calibrated SESR thresholds is presented in Sect 2.3.6.

2.3.1 Spatial and temporal sampling design

The period of analysis was from February to August from 2000-2024. February to April is considered an early warning opportunity period, since early evaporative stress signals during these months may condition soil moisture availability before the sowing period. April is a critical pre-sowing month, as high evaporative stress during this month can reduce germination success ahead of sowing. Farmers typically prepare the land and make sowing decisions (Verbist et al., 2018). Sowing typically occurs in May, with the main growing stages of maize and beans in June-July, while August is the end of the main cropping cycle. To represent the spatial dimension sample locations are distributed across six soil texture classes in rainfed areas (see Figure S1), allocated proportionally to ensure a representative sample in each soil texture class, resulting in a sampling interval of about 3 km and 388 time series of 8-day SESR values.

https://doi.org/10.5194/egusphere-2026-1010
Preprint. Discussion started: 10 March 2026

2.3.2 Impact benchmarks of drought-induced crop losses

Two agricultural-impact benchmarks related to drought-induced crop losses were created: one based on Vegetation Health Index (VHI) and a second derived from newspapers and reports (Figure 2). The VHI-based benchmark was used to identify impact-relevant years for calibration, whereas both benchmarks were used to validate literature-based and calibrated SESR thresholds. The benchmarks were obtained as follows:

(i) Years with drought-induced crop losses were obtained from the Vegetation Health Index (FAO, 2014). Crop losses were detected when VHI values at the end (in August) of the first cropping cycle fell below 0.35 (Fuganti et al., 2020). This criterion was applied independently at each sample location, each represented by independent time series. The resulting time series were then grouped by soil texture classes. Note that Figure 2 indicates the occurrence of crop loss impacts at one sample location and does not necessarily imply region-wide impacts.

(ii) Years with drought-induced crop loss reports were obtained from the two main national newspapers, as well as from the GIEWS, FEWS NET, and EM-DAT databases. Digital archives were systematically searched using drought- and impact-related keywords in Spanish and English, including "drought", "sequía", "lack of rain", "falta de lluvia", "lluvias tardan en llegar", "crop loss (es)", "pérdida de cosecha", "yield reduction", and combinations of these terms. For each candidate newspaper article or report, the information was organized into three levels of detail, each presented separately. The first level includes the date and a short description of the reported impacts for each source. The second level provides the dates, the type of impacts reported (e.g. economic, agricultural, population affected), and the sources. The third level summarizes the year, the crop impacts, and the sources reporting those impacts. Documented drought-induced crop loss events were retained only when reported by at least three independent sources. With respect to timing, newspapers usually report drought-related impacts from July onwards in the same year as the drought event occurs, which is the middle of the main cropping cycle under study. However, some international reports are reported in the year after the drought event. To harmonise the timing of reported impacts, each reported event was constrained to a one-month window centred on September. Crop losses reported between January and April were interpreted as impacts of drought events that occurred in the previous year. From a spatial perspective, crop loss impacts were inconsistently documented and spatially heterogeneous across municipalities and, consequently, across soil texture classes within the study area. Therefore, the drought-induced crop loss was interpreted as representative of broader regional conditions rather than as spatially explicit observations at the soil texture scale.

https://doi.org/10.5194/egusphere-2026-1010
Preprint. Discussion started: 10 March 2026

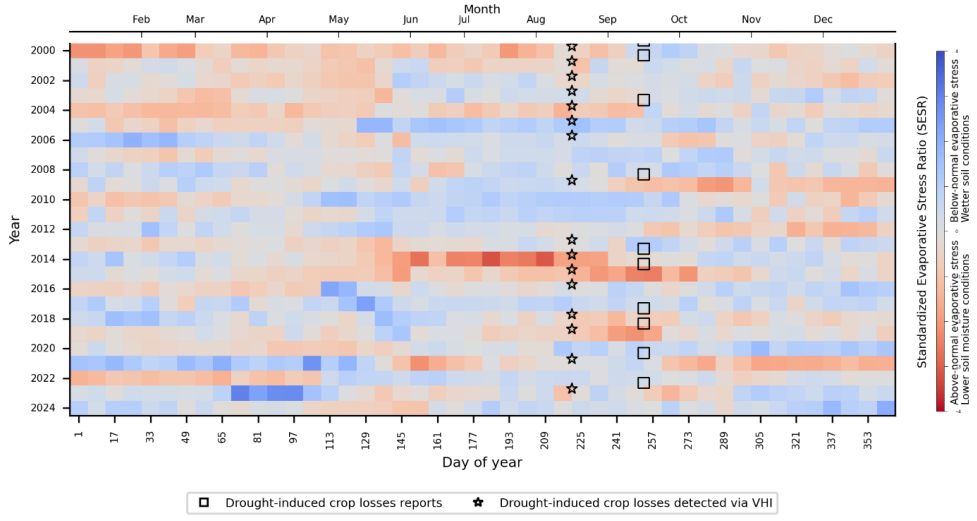

Figure 2 Years with crop losses derived from the Vegetation Health Index and reports at one representative sample location within the study area characterise by moderately fine clay-loam soil. The heatmap represents the median of the Standardized Evaporative Stress Ratio (SESR) across the sampled locations and aggregated at each 8-day interval.

2.3.3 Detection of agricultural flash droughts

In the Standardized Evaporative Stress Ratio (SESR) framework described by Christian et al., (2019), a flash drought event is identified using percentile thresholds applied to SESR and the rate of change of SESR (ΔSESR), together with a minimum duration requirement. Drought is classified when SESR falls below the 20th percentile of the distribution of SESR values, and the event becomes a flash drought when rapid and sustained intensification of evaporative stress persists for about 30 days. The rapid intensification is detected when ΔSESR crosses the 40th percentile of the distribution of ΔSESR values and when the average ΔSESR during the entire event remains below the 25th percentile. These thresholds have been equally applied in other studies (cf. Gou et al., 2022; Nguyen and Choi, 2024). This study refines this framework by replacing the fixed 20th percentile threshold with a calibrated threshold specific to crop management periods and soil texture.

When drought conditions are sustained, they signal an increase in evaporative stress, which in turn raises the likelihood of soil moisture decline and associated agricultural impacts. Based on this rationale, agricultural flash droughts (AFDs) in this study were detected when SESR dropped below a defined threshold ($\theta^*_{t,s}$), accompanied by an intense and sustained evaporative stress confirmed using the 40th and 25th percentile thresholds of the ΔSESR (Christian et al., 2019). Accordingly, an AFD was defined as:

$$AFD_{t,k=}\begin{cases}1, & if\ SESR_{t,s} \le \theta_{t,k} \wedge \Delta SESR_{t,k} \le P_{40}\ (1\ exeption\ allowed) \wedge \overline{\Delta SESR}_{AFD,p} \le P_{25}\\ 0, & Otherwise\end{cases} \quad (3)$$

Where $AFD_{t,k}$ denotes the presence (1) or absence (0) of an agricultural flash drought. $SESR_{t,k}$ is the Standardized Evaporative Stress Ratio across crop management period t and sample k falling in soil texture. $\theta_{t,k}$ is the SESR threshold to be calibrated. $\Delta SESR_{t,k}$ is the change of SESR between consecutive time intervals. P_{40} is the 40th percentile of ΔSESR values. P_{25} is the

https://doi.org/10.5194/egusphere-2026-1010
Preprint. Discussion started: 10 March 2026

25th percentile threshold of ΔSESR. $\overline{\Delta SESR}_{AFD,p}$ is the mean ΔSESR over the full agricultural flash drought period. ∧ denotes the logical "and " condition.

Figure 3 illustrates an agricultural flash drought (AFD) event in 2014 in fine clay-loam soil at one of the sample points. Panel (a) shows the SESR trajectory (black line) together with the calibrated threshold (red dashed line). From mid-May to early July, SESR dropped below the calibrated thresholds for 49 consecutive days. Panel (b) provides the ΔSESR during the event. Rapid intensification is confirmed when consecutive ΔSESR values remained below the 40th percentile, with only one exception allowed, which is marked here with an orange circle. The mean (μ) of the ΔSESR across the event also remained below the 25th percentile, reinforcing its classification as an AFD. In the figure, the actual μ(ΔSESR) and the 40th and 25th percentiles of the time series are shown to better illustrate the example. Detection therefore requires both sustained low SESR and rapid intensification, with the calibrated SESR threshold governing the event onset in this example.

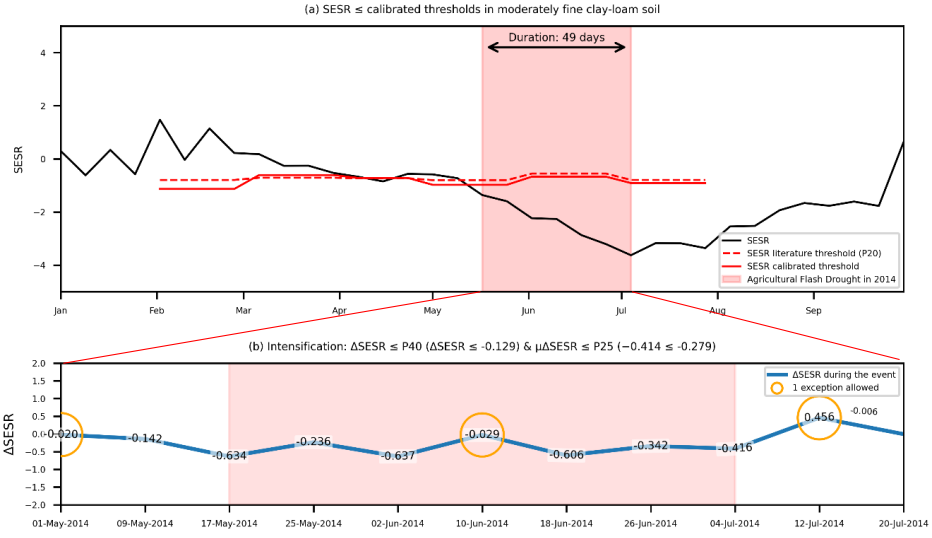

Figure 3 Time-series schematic showing how calibrated SESR thresholds and rapid intensification of SESR are used to detect agricultural flash drought in 2014. (a) SESR evolution relative to the literature-based threshold (P20) and the calibrated threshold ($\theta_{t,k}$). The shaded period indicates the detected agricultural flash drought, which begins when SESR first falls below the calibrated threshold (On May 17) and persists until recovery due to the criteria for ΔSESR being above the representative threshold. (b) Corresponding changes of SESR (ΔSESR) during the same period, used to confirm rapid intensification.

2.3.4 Diagnostic assessment of the agricultural relevance of SESR prior to calibration

Three diagnostic assessments were conducted to assess whether SESR functions as a potential agricultural indicator of evaporative stress linked to drought-induced crop losses. The first assessment examines the consistency between SESR and Vegetation Health Index (VHI) using aggregated data from all soil textures across the sample locations. To achieve this, a linear regression and Pearson correlation analyses were performed between SESR and VHI using two representative years: one with confirmed crop losses caused by drought and one with no reported losses.

https://doi.org/10.5194/egusphere-2026-1010
Preprint. Discussion started: 10 March 2026

The second assessment analyses the distribution of evaporative stress across crop management periods and soil texture classes. Its aim is to determine whether evaporative stress (SESR) differs between years with drought-induced crop losses and non-drought years when no losses occurred, with the VHI benchmark used to identify years with drought-induced crop losses. For each sample location the SESR time series were extracted in their original 8-day resolution for the period from February to July. Two datasets of SESR values were then created, one for years with and one for years without drought-induced crop losses. The distribution of the SESR values were visualised using boxplots by crop management periods and soil texture classes. As most SESR distributions deviated from normality (tested using Shapiro–Wilk normality test) (Ghasemi and Zahediasl, 2012), non-parametric tests, including Mann–Whitney U and Kolmogorov–Smirnov tests (Sawilowsky, 2005) were applied. Significant differences ($p < 0.05$) indicated that the SESR distributions differed between drought-induced crop loss and non-drought years.

2.3.5 Calibration of SESR thresholds, performance metrics, and uncertainty-based selection

The calibration aimed to identify SESR threshold values that best separate years with and without drought-induced crop losses by maximising the F_β score, thereby determining the evaporative stress associated with the occurrence of agricultural impacts. SESR threshold calibration was performed from 2000 to 2013 using SESR datasets constructed in Section 2.3.4, stratified by crop management periods and soil texture classes. Within each stratum, SESR observations were classified into two classes, positive and negative, corresponding to years with and without drought-induced crop losses. As the number of SESR time series (sample locations) were imbalanced between classes, inverse-frequency weighting was applied (Cao et al., 2019). Subsequently, these classes were used jointly during thresholds optimisation to evaluate candidate SESR thresholds. A set of candidate thresholds was defined as SESR values ranging between the second and ninety-fifth percentiles of the SESR distributions. For each candidate threshold, SESR values were converted into a binary classification distinguishing drought-impact conditions from non-impact conditions. These candidate thresholds were evaluated using an empirical-utility maximisation approach (Nan et al., 2012), in which thresholds were selected by maximising the F_β score ($\beta = 0.3$) for each crop management period and soil texture. For each candidate threshold, precision and recall were first computed and then the corresponding F_β score was derived. Precision represents the proportion of true positive results among all events classified as positive, whereas recall represents the proportion of true positive detections among all actual positive events in the data. The parameter β controls the relative weighting of precision and recall through the β^2 terms, with lower values (≤ 0.5) of β placing greater emphasis on precision and higher values (≥ 0.5) increasing the contribution of recall to the F_β score. The F_β metric is expressed as:

$$F_\beta = \frac{(1+\beta^2)\,P.\,R}{\beta^2\,P + R} \quad (4)$$

where P is precision, R is recall, and the F_β score represents an adjusted balance that weights P and R depending on the value of β. β is set to 0.3 to represent the preference of stakeholders for missed events over false alarms (Guimarães Nobre et al., 2023). During calibration, the tested candidate thresholds were explored using a 0.01 step size for fine exploration. A time step was classified as drought when the SESR value fell below the candidate threshold. To assess threshold robustness, the stability of the calibrated thresholds was evaluated by quantifying sampling uncertainty using cluster-level bootstrapping (Padiyedath Gopalan et al., 2019) with 1000 replicates (Efron and Tibshirani, 1986). The bootstrap was applied at the year–location level, resampling complete SESR time series (February-July) with replacement. Each bootstrap replicate produced an optimal threshold, and the resulting empirical distribution of calibrated thresholds was summarised using the median, standard deviation, and 95% confidence interval

https://doi.org/10.5194/egusphere-2026-1010
Preprint. Discussion started: 10 March 2026

(CI95%) to characterise variability and uncertainty. In addition to uncertainty assessment, the calibrated thresholds were also assessed using the false alarm rate (FAR) and Receiver Operating Characteristics Curve (ROC) and its Area Under Curve (AUC). Lower FAR values (≤ 0.2) indicate fewer false drought detections, whereas higher FAR values (≥ 0.5) indicate a higher frequency of false alarms. AUC values greater than 0.5 indicate that the thresholds provide discriminatory ability between years with and without drought-induced crop losses (Marzban, 2004). These performance and uncertainty metrics, together with the precision metric, were used to select the final set of calibrated thresholds, retaining only those values of thresholds as skilful that simultaneously satisfy the following criteria: precision ≥ 0.70, FAR ≤ 0.30, ROC-AUC ≥ 0.60, and CI95% ≤ 0.40. These criteria were chosen to approximate likely stakeholder preferences for reliable drought detection with limited false alarms, while maintaining acceptable discriminatory skill and stable thresholds estimates.

2.3.6 Validation strategy of literature-based and calibrated SESR thresholds

Using two validation metrics, the validation step assessed the ability of both literature-based and calibrated SESR thresholds to identify flash drought events for each crop management period and soil texture that coincide with years associated with drought-induced crop losses. The validation was performed only for the skilful thresholds identified during calibration, as described above. SESR thresholds validation was conducted from 2014 to 2024 using two distinct agricultural benchmarks: (1) drought-induced crop loss signals derived from the VHI and (2) documented historical drought-induced crop losses reported. The first validation metric (V_1) was defined as:

$$V_1 = \begin{cases} 1, & FD_t = 1 \; and \; cl_t = 1 \\ 0, & otherwise \end{cases} \quad (5)$$

Where V_1 represents the validation criterion, FD_t denotes a flash drought event identified at time t, and cl_t represents the crop loss condition at the end of the first cropping cycle (here, August). A second validation metric (V_2) was defined to assess whether flash drought events coincide with reported drought-induced crop losses:

$$V_2 = \begin{cases} 1, & \text{if } FD_t = 1 \; and \; dci_t = 1 \\ 0, & otherwise \end{cases} \quad (6)$$

Where V_2 represents validation criterion, and dci_t denotes documented drought-induced crop impacts for September, as defined in developing the impact benchmark.

3. Results

3.1 Agricultural relevance of the Standardized Evaporative Stress Ratio (SESR)

Figure 4 presents the regression equations and correlation coefficient that describe the relationship between SESR and VHI in both conditions for a year (2014) with and without (2013) drought-induced crop losses. Although the relationship between SESR and VHI is positive in both years, a smaller slope (b=1.49) and correlation (r=0.29) in 2013 indicate a weak relationship, while in 2014 the clearer slope (b =3.94) and correlation (r=0.63) suggest a stronger vegetation response to evaporative stress during drought years with confirmed crop losses. The distribution of SESR values at the lower VHI values indicates poor vegetation health and aligns with more negative SESR values, reflecting stronger evaporative stress. Although correlation does not imply causation, the fact that these differences emerge even in a naturally dry environment like the Dry Corridor indicates that SESR provides a meaningful signal that is coherent with vegetation stress during drought years with confirmed crop losses.

https://doi.org/10.5194/egusphere-2026-1010
Preprint. Discussion started: 10 March 2026

Boxplots of SESR distributions (Figure 5), together with the statistical difference tests (see Figure S2), illustrate how evaporative stress varies across crop management periods and soil textures between years with and without drought-induced crop losses. During February and March, SESR distributions exhibit strong overlap in both medians and interquartile ranges (IQRs), indicating limited separation between conditions. From April onwards, separation begins to emerge, with the clearest differences occurring in May–July, when years with drought-induced crop losses consistently show lower SESR medians across all soil textures. This separation is weakest in coarse sandy soils, where IQRs remain large and strongly overlapping. In contrast, it is strongest in finer-textured soils (moderately fine clay loam, fine clayey, and very expansive clayey), where a persistent downward shift in the median occurs without a corresponding increase in distributional spread. During June–July, separation further increases due to more frequent and more negative SESR values, particularly in fine-texture soils, indicating that the late period differences arise from both shifts in typical conditions (lower medians) and enhanced lower tail behaviour.

The relatively low discrimination of SESR in sandy soils between drought-induced crop loss years may be explained by their high permeability and low water-holding capacity (Jabro et al., 2009; Wankmüller et al., 2024), which cause rapid responses to evaporative demand even in years without crop losses. Consistent with this behaviour, statistical tests show no significant differences in SESR between years for sandy soils (Figure S2). In contrast, the stronger discrimination observed in clay-rich soils is likely linked to their higher water retention capacity (Or and Lehmann, 2019; Sun et al., 2019), which allows evaporative stress signals to persist longer and enhances the contrast in SESR between drought-induced crop loss and no-drought years. This separation is supported by statistically differences ($p < 0.05$) in both tests (Figure S2). Moreover, the upper and lower tails of the SESR distribution in these soils exhibit comparable lengths, indicating that the area experiences a balanced range of extreme transitions rather than being dominated exclusively by drying or wetting anomalies. This balance enables SESR to capture both the intensification and easing of evaporative stress, thereby supporting a more reliable identification of stress related thresholds.

https://doi.org/10.5194/egusphere-2026-1010
Preprint. Discussion started: 10 March 2026

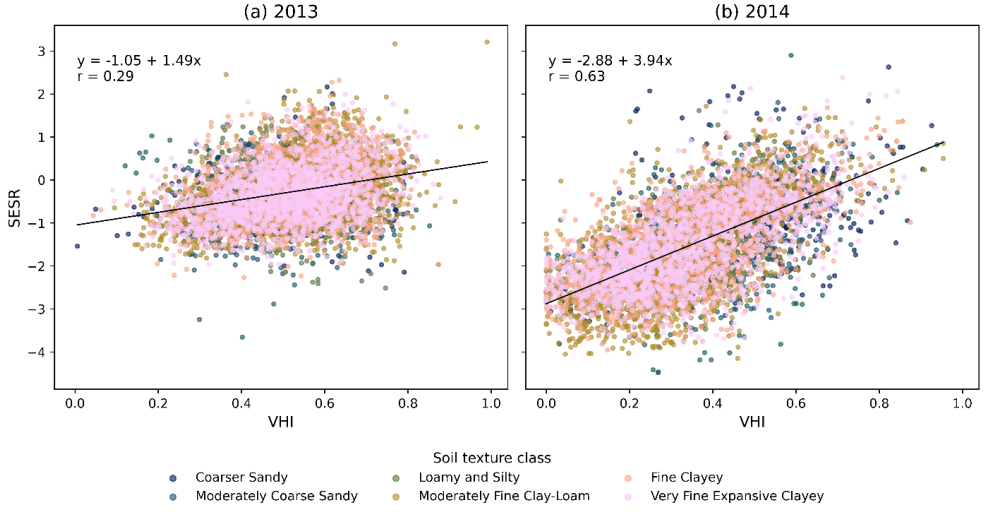

Figure 4. Scatterplots of the relationship between SESR and VHI from February to July in (a) 2013 (year without drought) and (b) 2014 (drought year with confirmed crop losses), with data aggregating across all soil textures at the sample locations. Each panel includes the fitted linear regression line, the regression equation (y), and the Pearson correlation coefficient (r).

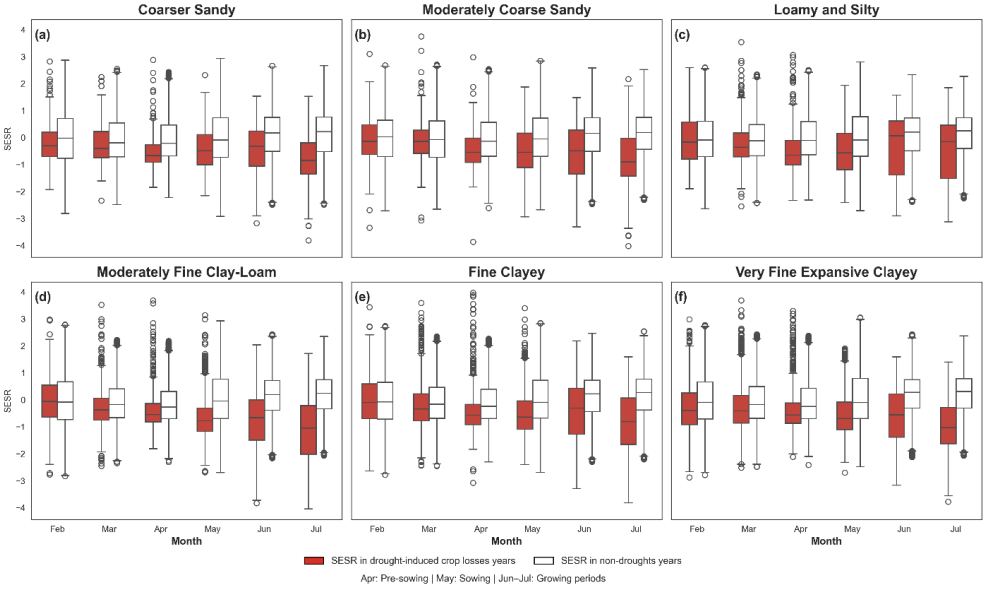

Figure 5 Panel (a)–(f) Standardized Evaporative Stress Ratio (SESR) aggregated across crop management periods and soil texture classes at the sample locations for years with and without drought-induced crop losses.

3.2 Performance of calibrated SESR thresholds across crop management period and soil textures

Figure 6 shows how the median performance metrics of precision, recall, FAR (False Alarm Rate) and F_β vary as the value of the thresholds $\theta_{t,k}$ (Eq. 3). This allows identification of the

https://doi.org/10.5194/egusphere-2026-1010
Preprint. Discussion started: 10 March 2026

thresholds for each crop management period and soil texture that achieves the best combination as expresed by F_β. In each panel, the calibrated threshold ($\theta_{t,k}$) is indicated by a soild vertical line, with the value indicated in the title. The literature-based threshold is shown as a dotted vertical line reference. While Figure 6 illustrates the overall median behaviour of the metrics across the thresholds range, the numerical values discussed below refer specifically to the values of the performance metrics at the calibarted thresholds. Figure 7 summarizes where SESR thresholds exhibit skill across periods and soils.

In all soil textures, higher values of the SESR thresholds increases recall and FAR and decreases precision. The metric combinations at the F_β maximum differ across soil textures and crop management periods. During the pre-sowing period (April), loamy and silty soils exhibit calibrated thresholds with balanced precision (≈0.83) and recall (≈0.68), while coarser sandy soils show lower recall (≈0.43−0.66) and higher FAR (>0.20). During the sowing period (May), most soils are characterised by calibrated thresholds with reduced recall (<0.45) and FAR typically bellow 0.12, including moderately coarse sandy, loamy–silty, and clay–loam soils. In contrast, during the growing period (June–July), calibrated thresholds in nearly all soil textures have high precision (>0.84) and low FAR (<0.12), while recall varies across soils, ranging from approximately 0.32 in coarser sandy soils to above 0.68 in fine and very fine clayey soils. Lower discriminaton skills is mainly observed during the pre-sowing (April), and sowing (May) periods for severals soil textures, including coarse sandy, moderately coarse sandy, and loamy–silty soils (AUC ≤ 0.70, Figure 7). In contrast, higher discrimination skill is consistently observed during the growing period (June–July) across most soils textures, with AUC values commonly exceedeing 0.80 and reaching above 0.90 in fine and very clayey soils for individual sample points.

https://doi.org/10.5194/egusphere-2026-1010
Preprint. Discussion started: 10 March 2026

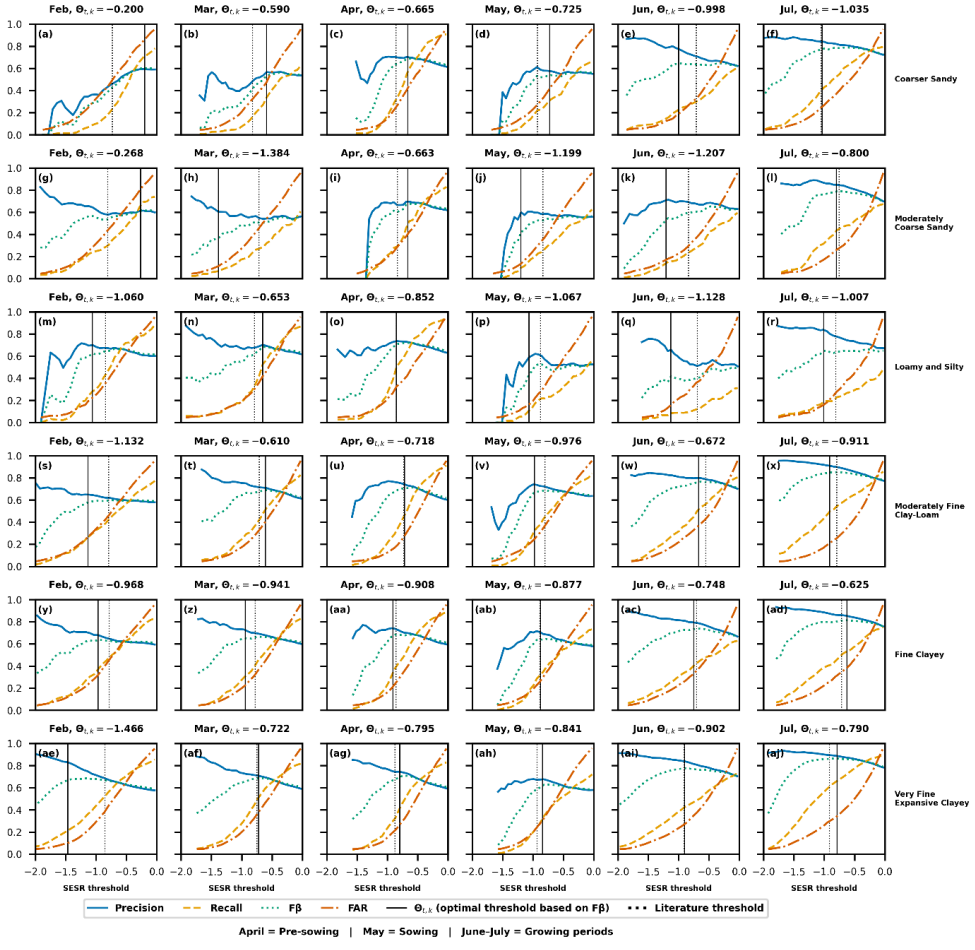

Figure 6 Median performance metrics of SESR thresholds across crop management periods and sample points for each soil texture, including precision, recall, F_β, and False Alarm Rate (FAR) evaluated over the full thresholds range. Solid vertical line denotes the optimal calibrated thresholds ($\theta_{t,k}$), while the dotted vertical line shows reference thresholds from literature. Note that the z-score of the literature thresholds is derived from the empirical distribution of SESR.

https://doi.org/10.5194/egusphere-2026-1010
Preprint. Discussion started: 10 March 2026

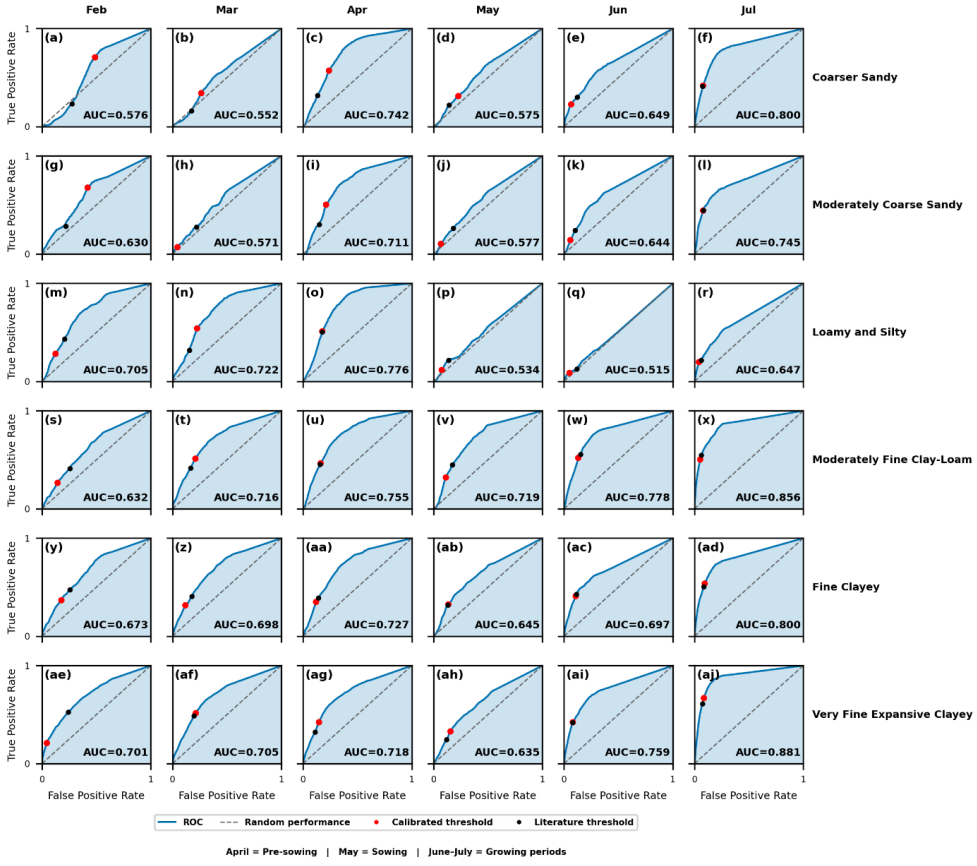

Figure 7 Median Receiver-Operating Characteristics Curve (ROC) values across crop management periods and sample points for each soil textures.

3.3 Stability and uncertainty of SESR thresholds

Figure 8 show the uncertainty in the optimal SESR-based thresholds across crop management periods and soil textures, expressed by the CI95 metric. Cells with a solid black outline indicate soil-month combinations for which the thresholds simultaneously satisfy the predefined criteria: precision ≥ 0.70, FAR ≤ 0.30, ROC-AUC ≥ 0.60, and CI95% ≤ 0.40. Only these thresholds were retained for validation.

Threshold uncertainty varies across both crop management periods and soil textures. Sandy soils (coarse sandy and moderately coarse sandy) exhibit the highest CI95 range during the selected period. In contrast, intermediate and fine-textured soils show lower CI95 range. Skilful thresholds are identified for loamy and silty soils during March and April (pre-sowing period), for moderately fine clay-loam soils during April and June–July (growing period), and for very expansive clayey soils from March through July (growing period). Fine clayey soils show intermediate uncertainty, with CI95 ranges exceeding the selection threshold in most months. Figure S3 illustrates the full distribution of the calibrated SESR thresholds.

https://doi.org/10.5194/egusphere-2026-1010
Preprint. Discussion started: 10 March 2026

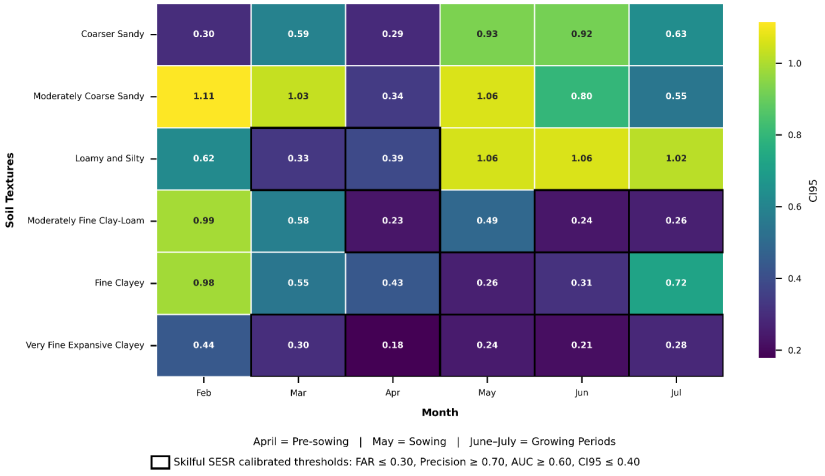

Figure 8 Uncertainty level of optimal thresholds by crop management periods and soil textures. The black cell shows the optimal thresholds that simultaneously satisfied the following criteria: precision ≥ 0.70, FAR ≤ 0.30, ROC-AUC ≥ 0.60, and CI95% ≤ 0.40.

3.4 Validation of literature-based and calibrated SESR thresholds

Figure 9 illustrates years in which flash droughts are detected using calibrated thresholds and literature-based thresholds for the validation period (2014-2024), and how these align against years with crop losses. This shows that flash drought events that are detected using calibrated thresholds appear in more years and across more soil textures than those detected using literature-based thresholds. In moderately fine clay-loam, fine clayey, and very fine expansive clayey soils, calibrated thresholds detections are present in several years in which crop losses are also shown. In contrast, detections based on literature thresholds are absent or limited to fewer years for these same soils. In loamy and silty soils, both calibrated and literature-based flash drought detections occur less frequently, and several years with crop losses do not show a corresponding flash drought detection. Across all soil textures, there are also years in which flash drought detection occur without accompanying crop losses, and years in which crop losses occur without flash drought detections. Supplementary Figures S4 and S5 summarise the hit rates between flash droughts detected using literature (column left) and calibrated-based thresholds versus crop losses detected via VHI and reports. For all soil textures, hit rates are zero or low during the pre-sowing and sowing periods. During the growing period (June–July), calibrated thresholds yield consistently higher hit rates than literature-based thresholds across all soil textures, with the highest values observed in moderately fine clay-loam and fine clayey soils. In contrast, hit rates associated with literature-based thresholds remain low across all periods and soil textures.

https://doi.org/10.5194/egusphere-2026-1010
Preprint. Discussion started: 10 March 2026

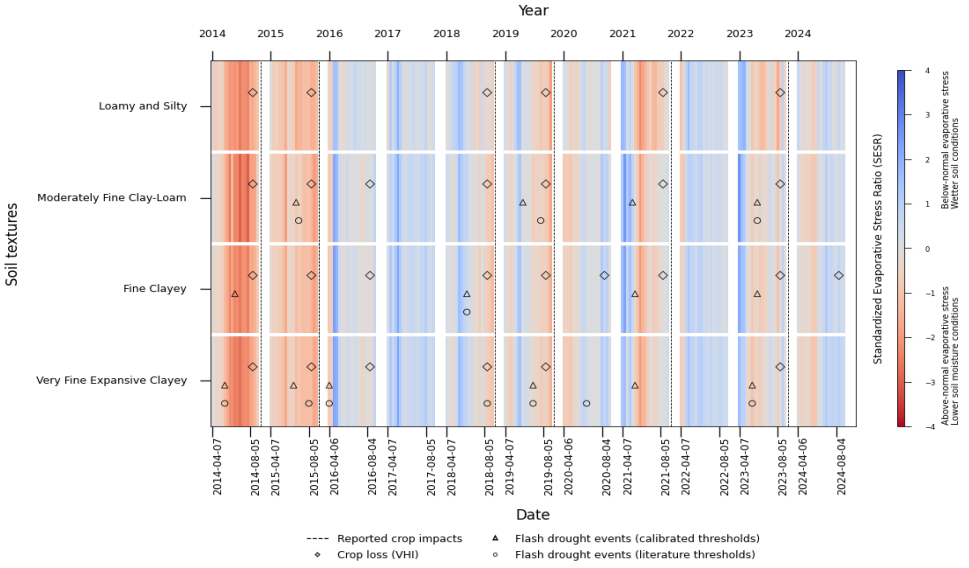

Figure 9 Temporal alignment of flash droughts events and crop losses identified via VHI and newspapers/reports. The 8-day SESR time series for each soil texture is shown as the background over the evaluation period. Flash drought events detected using calibrated and literature-based thresholds, together with reported crop losses, are overlaid.

4. Discussion

4.1 Relevance of SESR in detecting agricultural flash droughts

Results show that the Standardized Evaporative Stress Ratio (SESR) captures a coherent signal of higher evaporative stress during years in which crop losses are observed, as indicated by contrasts in the SESR-VHI relationship between non-drought and drought years (Figure 4). This indicates that SESR is coherent with vegetation stress during years with confirmed crop losses, and consistent with the mechanism whereby vegetation becomes increasingly sensitive to evaporative stress once soil moisture constraints emerge, while under non-limiting conditions changes in evaporative demand do not translate into physiological stress (Anderson et al., 2016; Hobbins and Huntington, 2016; Kozlowski, 1968). However, translating this signal into an indicator of agricultural flash drought depends on how the onset threshold is defined within the detection approach (Section 2.3.3). Analysis of the distribution of SESR values (Figure 5) shows that more extreme SESR values occur during years with drought-induced crop losses. Although literature-based and calibrated thresholds are derived separately for each crop management period and soil texture, they approach similar values in a limited number of cases (Figure 6), this behaviour is not consistent across soil textures and crop management periods. This inconsistency arises because literature-based thresholds are defined solely by the statistical properties of the SESR distribution (Christian et al., 2019), whereas calibrated thresholds are constrained by the occurrence of observed crop losses (see sections 2.3.2, 2.3.3, 2.3.5), leading to different SESR values being identified as agriculturally relevant even within the same soils texture and management period. In the dry corridor of Central America, drought-induced crop losses occur at SESR levels that depend on this approach rather than on percentile exceedance alone (see

https://doi.org/10.5194/egusphere-2026-1010
Preprint. Discussion started: 10 March 2026

Figures S4, S5). Consequently, calibrating using agricultural impact information improves the consistency in which SESR identifies agriculturally relevant flash droughts, compared to the use of fixed percentile threshold alone (Section 2.3.5).

This limitation in how flash drought onset is defined also has direct operational consequences for the alignment between detected events and observed crop losses. The default threshold ignores agricultural context and cannot be directly linked to the occurrence of crop losses. When detection occurs outside pre-sowing, sowing and growing periods, its operational value is limited (Bucheli et al., 2021), meaning that the occurrence of flash drought may then not correspond to crop losses (Teleubay et al., 2025), consistent with the low hit rates in Figures S4-S5. These limitations are reflected in the less consistent temporal alignment between literature-based detections and documented crop losses years, compared to the calibrated thresholds (Figure 9). Together, the results demonstrate that SESR provides signals of evaporative stress relevant for agricultural flash drought detection, but that in this dryland system such relevance requires context-specific, impact informed calibration rather than fixed percentile thresholds (Halwatura et al., 2017). These finding are also with a core principle of impact-based forecasting, namely that hazard signals must be translated into locally relevant impact thresholds to support meaningful early warning and decision-making (McEwen et al., 2021; Shyrokaya et al., 2024).

4.2 Behaviour of calibrated SESR thresholds across soil textures and crop management periods to detect agricultural flash droughts

The response of calibrated SESR thresholds across soil textures and crop management periods shows that flash drought detection depends on both the temporal evolution of evaporative stress and the capacity of each soil texture to store and release moisture during crop management periods. In the Dry Corridor in Nicaragua, high atmospheric demand marked by the transition between the dry season and the rainy season produces rapid fluctuations in soil moisture (Son et al., 2018). Because local maize and bean systems rely almost entirely on precipitation (van der Zee Arias et al., 2012), these moisture fluctuations coincide with short-term stress conditions that are reflected in SESR variability during drought years (Figure 5), thereby shaping the variability of SESR signals used for onset detection.

Coarse and moderately sandy soils, with rapid drainage and low water capacity (Jabro et al., 2009; Wankmüller et al., 2024), generate short-lived and highly variable evaporative stress. As a result, SESR anomalies are less persistent and less clearly associated with crop losses, making the distribution of SESR values (Figures 5a,b) difficult to discriminate between years with and without identified crop losses (Figure 2), and resulting in calibrated thresholds characterised by high uncertainty (Figure 8). In contrast, clay-rich soils, characterised by greater water retention and slower drainage (Jabro et al., 2009), allow evaporative stress to persist over longer periods (Suliman et al., 2024; Wankmüller et al., 2024), which is reflected in the more stable calibrated thresholds in several clay soil classes and periods (Figure 8). Loamy–silty soils, which have intermediate porosity and water-holding capacity (Ma et al., 2015), exhibit a more mixed behaviour. Although they show clear separation of the SESR signal during pre-sowing, sowing and growing periods (Figure 5c), calibrated SESR thresholds for loamy–silty soils do have skill in the sowing month (Figure 8). These contrasts indicate that SESR-based detection is most reliable where soil moisture deficits persist long enough to affect crops, whereas rapidly draining soils reduce the operational usefulness of SESR as a standalone indicator.

https://doi.org/10.5194/egusphere-2026-1010
Preprint. Discussion started: 10 March 2026

The usefulness of calibrated SESR thresholds is governed not only by soil texture but also by the seasonal progression of evaporative stress across crop management periods (Son et al., 2018). During the dry season months that precede the sowing period, high evaporative stress dominates the SESR signal (Noguera et al., 2022; Otkin et al., 2018), producing large variability that often reflects background seasonal drying rather than short-term stress anomalies associated with agricultural impacts (Hobbins and Huntington, 2016). Under these conditions, SESR anomalies may reflect seasonal atmospheric demand rather than crop relevant moisture stress, reducing the reliability of thresholds-based detection. The effect of this background drying on detection performance differs by soil texture. In sandy soils, this short-lived evaporative stress variability produces high false alarm rates (FAR) and weak discrimination in some months (Figure 7), together with the wide uncertainty ranges in calibrated thresholds (Figure 8).

Once precipitation begins to moderate evaporative stress (see SESR heatmap across years and months aggregated at each 8-day interval in Figure 2) in the sowing period in May and during the growing period in July for maize and beans (Figure 1), soil moisture is replenished more regularly (Son et al., 2018), which reduces the gap between ET and PET (Hobbins et al., 2019) and also reduces short-term variability in SESR (Noguera et al., 2022). Under these more stable conditions, SESR anomalies can more clearly reflect crop relevant moisture deficits in the soil-period combinations where skilful detection is observed (Anderson et al., 2016). This seasonal transition modifies the SESR signals, but ROC results indicate that skilful discrimination does not increase uniformly after rainfall onset (Figure 7). Instead, skill emerges only in specific soil period combinations, reflecting the interaction between seasonal moisture dynamics and soil water holding capacity. Operationally, this implies that SESR-based flash drought monitoring in dryland agricultural systems should focus on the specific soil-period combinations where skilful detection is observed, rather than applying a uniform approach across all soil textures and months.

4.3 Operational relevance and limitations of calibrated SESR thresholds for flash drought monitoring and management

The calibrated thresholds reveal context-dependent limitations that must be recognised when integrating SESR into operational drought monitoring. In sandy soils, SESR shows limited ability to distinguish anomalous evaporative stress from background dryness signals (Hobbins and Huntington, 2016; Jabro et al., 2009), resulting in low detection skill and high uncertainty in calibrated thresholds. On the other hand, the skilful thresholds occur predominantly in clay-rich soils, which account for around ~90% of the study area (Figure 1), during pre-sowing, sowing, and growing periods and only during pre-sowing period in loamy–silty textures (Figure 8). This spatial and temporal concentration of skilful thresholds indicates that SESR provides operational value only for specific combinations of crop management period and soil texture, and that its performance cannot be assumed outside these domains. Therefore, SESR-based monitoring could not be suitable as a uniformly applied early warning tool across all periods and soils, but rather as a selective component restricted to the conditions where calibrated thresholds demonstrate stability and skill. Even in these settings, SESR-based detections would benefit from verification using complementary information, such as soil moisture indicators, land surface temperature or field-based agronomic observations, to confirm or filter detections (Torelló-Sentelles and Franzke, 2022), and to avoid overinterpreting SESR signals in such settings, as documented in previous studies in dryland regions such as located in Central America (Kibler et

https://doi.org/10.5194/egusphere-2026-1010
Preprint. Discussion started: 10 March 2026

al., 2023; Quichimbo et al., 2021; Sun et al., 2019). Additionally, the operational relevance of SESR thresholds depends on the trade-off between high recall and low precision that local governments, managers and farmers are willing to accept (Guimarães Nobre et al., 2023). The choice of the optimal threshold based on the maximum value of F_β is conditioned by the parameter β, which determines how the system balances missed events and false alarms (Gallear et al., 2025). In this study, thresholds were selected to favour precision, consistent with a context where false alarms carry high costs (Guimarães Nobre et al., 2019) and institutional response capacity is limited. Under this configuration (β= 0.3), the optimal threshold shifts towards more negative values. This reduces false alarms (FAR) but increases the likelihood of missing early flash drought development. When β = 1, which prioritises recall, thresholds shift toward less negative SESR values, increasing detection under weaker stress and thereby increasing FAR. This behaviour of SESR as an indicator is consistent with findings with other indicators in Halwatura et al., 2017; Gallear et al., 2025; Torelló-Sentelles and Franzke, 2022. As discussed in the literature, decision-makers often avoid acting when uncertainty is high, because the penalties associated with false alarms are visible, whereas the benefits of early actions are less immediately apparent (Bailey, 2012).

These decision rules ultimately depend on local decision-makers needing to prioritise (Guimarães Nobre et al., 2019; Lopez and Haines, 2017), and in the rainfed dry corridor of Central America, this statistical trade-off translates directly into an economic one. By mid-May, farmers have already committed financial resources—loans, fertiliser, purchases and labour—(van der Zee Arias et al., 2012). Because flash droughts typically evolve over timescales comparable to the sowing period (~30 days), prioritising precision may reduce false alarms (Gallear et al., 2025) but delay response, thus limiting the opportunity to reschedule planting or implement mitigation (Solh and van Ginkel, 2014). Conversely, favouring recall in May may increase early detection even under weak stress signals (Halwatura et al., 2017) and enable preventive action, but at potentially high implementation costs. In line with principles discussed in the impact-based forecasting (Shyrokaya et al., 2024), a more appropriate strategy would be to redefine the objective function according to economic risk (Bailey, 2012; Portele et al., 2021; Salmoral et al., 2019) and cost-loss analysis (Zhu et al., 2002), as well as the participation of stakeholders rather than purely statistical criteria (McEwen et al., 2021). Although this study dynamically adjusted the optimal thresholds to reflect the spatial and temporal variability, considering crop management periods and soil textures, fully operational deployment would require extending this approach to explicitly account for economic risk and decision-making constraints.

5. Conclusions

In this study, a context-specific threshold calibration approach was developed to improve the spatial and temporal detection of agricultural flash drought conditions in support of drought monitoring and management. The study was conducted in the Central America Dry Corridor, a dryland region in Nicaragua that is representative of rainfed agricultural systems exposed to short-lived but intense evaporative stress found in many tropical drylands worldwide. The approach uses the Standardized Evaporative Stress Ratio (SESR), together with its rate of change (ΔSESR), and calibrates SESR thresholds using two benchmarks of observed drought-induced crop loss impacts. Calibrated SESR thresholds were evaluated across crop management periods and soil textures. The conclusions are summarised below:

https://doi.org/10.5194/egusphere-2026-1010
Preprint. Discussion started: 10 March 2026

- Although SESR contains coherent signals of evaporative stress intensification during years with drought-induced crop losses, default thresholds used in the literature do not translate this signal into a useful indicator of agricultural relevance. These default thresholds frequently identify stress conditions in years without reported losses while failing to capture the more extreme SESR values at which agricultural impacts are observed in this dryland context. As a result, literature-based thresholds show limited suitability for operational flash drought monitoring in the study region.

- Calibrated thresholds reveal that the detectability of agriculturally relevant flash drought conditions using SESR depends jointly on crop management periods and soil textures. Skilful thresholds could not be found in sandy soils, where rapid soil moisture fluctuations limit the persistence of evaporative stress signals rather than the occurrence of agricultural impacts themselves. In contrast, clay-rich soils exhibit stable and skilful thresholds during specific crop management periods within pre-sowing, sowing and growing periods (April to July), with the skilful months varying among individual clay-rich soils classes. Loamy–silty soils showed intermediate behaviour, with skilful thresholds only in March and the pre-sowing period in April. These results indicate that SESR-based flash drought detection cannot be generalised uniformly across space or time but instead depends on the interaction between soil hydraulic properties and seasonal evolution of evaporative stress.

- Validation against the agricultural benchmarks confirms that calibrated thresholds detect flash drought conditions more frequently in years that also exhibit drought-induced crop losses than literature-based thresholds, while still producing detections in some years without reported losses and missing impacts in others. This indicates that SESR thresholds can provide operationally relevant but conditional information, with useful performance confined to specific soil-crop management period combinations, particularly during the growing period, where threshold stability and detection skill are jointly satisfied. More broadly, these findings support ongoing effort toward impact-based drought monitoring and early warning by showing that physically based indicators such as SESR require calibration against observed agricultural impacts to be operationally meaningful. Rather than assuming that evaporative stress thresholds alone are sufficient to indicate agricultural impacts, this study demonstrates that linking SESR-based stress signals to crop losses and crop management periods improves their relevance for agricultural decision-making. At the same time, the results highlight that fixed percentile thresholds are insufficient in heterogeneous dryland environments, where translation from physical stress to agricultural impact is strongly context dependent.

This research provides temporally and spatially calibrated thresholds for agricultural flash drought detection in the Central America Dry Corridor, further work is needed to generalise and deepen these findings. As the approach itself is generalisable, future research should test the skill of flash drought detection using calibrated thresholds in other dryland regions and cropping systems. Additionally, further research should explore adding complementary variables in settings where SESR alone does not sufficiently discriminate impact-relevant stress conditions. Finally, threshold selection cannot be reduced to mechanical optimisation of statistical metrics; effective operational use requires explicit consideration of economic risk, stakeholder priorities, and the asymmetric consequences of missed events and false alarms so that SESR-based alerts support timely, informed, and context-appropriate decision-making for farmers and institutions.

https://doi.org/10.5194/egusphere-2026-1010
Preprint. Discussion started: 10 March 2026

6. Data availability and code

The data and code are available on request.

7. Author contributions

IU-T: conceptualisation (lead), methodology (lead), investigation (lead), formal analysis (lead), data curation and coding (lead), visualisation (lead), writing original draft, review and editing (lead), funding acquisition (lead). MW: conceptualisation (lead), methodology (lead), and supervision (lead). CB and MC, conceptualisation (supporting), methodology (supporting), supervision (supporting), GJ: conceptualisation (supporting), methodology (supporting), supervision (supporting), funding acquisition (lead). The first draft was written by IU-T, and all authors commented on previous versions of the manuscript.

8. Competing of interests

The author declares that none of the authors has any competing interests.

9. Acknowledgments

The author thanks the Schlumberger Foundation Faculty for the Future Fellowship Program for their financial support.

10. Financial support

This work was financially supported by the Schlumberger Foundation Faculty for the Future Fellowship Program.

11. Bibliography

Anderson, M. C., Zolin, C. A., Sentelhas, P. C., Hain, C. R., Semmens, K., Tugrul Yilmaz, M., Gao, F., Otkin, J. A., Tetrault, R. The evaporative stress index as an indicator of agricultural drought in Brazil: an assessment based on crop yield impacts, Remote Sens. Environ., 174, 82–99, https://doi.org/10.1016/j.rse.2015.11.034, 2016.

Bailey, R. Famine early warning and early action: the cost of delay. Chatham House, London, 24 pp., 2012.
https://www.chathamhouse.org/sites/default/files/public/Research/Energy,%20Environment%20and%20Development/0712pr_bailey.pdf

Basara, J. B., Christian, J. I., Wakefield, R. A., Otkin, J. A., Hunt, E. H., Brown, D. P. The evolution, propagation, and spread of flash drought in the Central United States during 2012, Environ. Res. Lett., 14, 084025, https://doi.org/10.1088/1748-9326/ab2cc0, 2019.

Bucheli, J., Dalhaus, T., Finger, R. The optimal drought index for designing weather index insurance, Eur. Rev. Agric. Econ., 48, 573–597, https://doi.org/10.1093/erae/jbaa014, 2021.

Buitink, J., van Hateren, T. C., Teuling, A. J. Hydrological system complexity induces a drought frequency paradox, Front. Water, 3, 640976, https://doi.org/10.3389/frwa.2021.640976, 2021.

Cao, K., Wei, C., Gaidon, A., Arechiga, N., Ma, T. Learning imbalanced datasets with label-distribution-aware margin loss, Adv. Neural Inf. Process. Syst., 32, 1567–1578, 2019.

Christian, J. I., Basara, J. B., Otkin, J. A., Hunt, E. D., Wakefield, R. A., Flanagan, P. X., Xiao, X. A methodology for flash drought identification: application of flash drought frequency

https://doi.org/10.5194/egusphere-2026-1010
Preprint. Discussion started: 10 March 2026

772 across the United States, J. Hydrometeorol., 20, 833–846, https://doi.org/10.1175/JHM-D-18-
773 0198.1, 2019.

774 DGOT–INETER. Atlas nacional de suelos de la República de Nicaragua. Managua, Nicaragua,
775 2024. https://www.ineter.gob.ni/mapa/pub/atlassuelo/1erAltasNacionaldeSuelos.pdf

776 Edris, S. G., Basara, J. B., Christian, J. I., Hunt, E. D., Otkin, J. A., Salesky, S. T., Illston, B. G.
777 Analysis of the critical components of flash drought using the standardized evaporative stress
778 ratio, Agric. For. Meteorol., 330, 109288, https://doi.org/10.1016/j.agrformet.2022.109288,
779 2023.

780 Efron, B., Tibshirani, R. Bootstrap methods for standard errors, confidence intervals, and other
781 measures of statistical accuracy, Stat. Sci., 1, 54–75, https://doi.org/10.1214/ss/1177013815,
782 1986.

783 FAO. Vegetation health index near real time (Global - dekadal - 1 km) - ASIS (raster), FAO,
784 2014. https://www.fao.org/giews/earthobservation/access.jsp

785 Fuganti, G., Minelli, M., Rojas, O. Practical guidelines for early warning–early action plans on
786 agricultural drought. FAO, Rome, Italy, 2020. https://openknowledge.fao.org/items/dd8ad74b-
787 8c2f-40e6-b899-62e52d2aad07

788 Gallear, J. W., Valadares Galdos, M., Zeri, M., Hartley, A. Evaluation of machine learning
789 approaches for large-scale agricultural drought forecasts to improve monitoring and
790 preparedness in Brazil, Nat. Hazards Earth Syst. Sci., 25, 1521–1541,
791 https://doi.org/10.5194/nhess-25-1521-2025, 2025.

792 Ghasemi, A., Zahediasl, S. Normality tests for statistical analysis: a guide for non-statisticians,
793 Int. J. Endocrinol. Metab., 10, 486–489, https://doi.org/10.5812/ijem.3505, 2012.

794 Gou, Q., Zhu, Y., Lü, H., Horton, R., Yu, X., Zhang, H., Wang, X., Su, J., Liu, E., Ding, Z.,
795 Wang, Z., Yuan, F. Application of an improved spatio-temporal identification method of flash
796 droughts, J. Hydrol., 604, 127224, https://doi.org/10.1016/j.jhydrol.2021.127224, 2022.

797 Gu, Y., Wylie, B. K., Howard, D. M., Phuyal, K. P., Ji, L. NDVI saturation adjustment: a new
798 approach for improving cropland performance estimates in the Greater Platte River Basin,
799 USA, Ecol. Indic., 30, 1–6, https://doi.org/10.1016/j.ecolind.2013.01.041, 2013.

800 Guimarães Nobre, G., Davenport, F., Bischiniotis, K., Veldkamp, T., Jongman, B., Funk, C.
801 C., Husak, G., Ward, P. J., Aerts, J. C. J. H. Financing agricultural drought risk through ex-ante
802 cash transfers, Sci. Total Environ., 653, 523–535, 653, 523–535,
803 https://doi.org/10.1016/j.scitotenv.2018.10.406, 2019.

804 Guimarães Nobre, G., Pasqui, M., Quaresima, S., Pieretto, S., Lemos Pereira Bonifácio, R. M.
805 Forecasting, thresholds, and triggers: towards developing a forecast-based financing system for
806 droughts in Mozambique, Clim. Serv., 30, 100344,
807 https://doi.org/10.1016/j.cliser.2023.100344, 2023.

808 Halwatura, D., McIntyre, N., Lechner, A. M., Arnold, S. Capability of meteorological drought
809 indices for detecting soil moisture droughts, J. Hydrol.: Reg. Stud., 12, 396–412,
810 https://doi.org/10.1016/j.ejrh.2017.06.001, 2017.

https://doi.org/10.5194/egusphere-2026-1010
Preprint. Discussion started: 10 March 2026

Hobbins, M. T., Huntington, J. L. Evapotranspiration and evaporative demand. In: Singh, V. P. (Ed.), Handbook of applied hydrology, 2nd ed., McGraw-Hill Education, New York, USA, 42.1–42.18, 2016.

Hobbins, M., Dewes, C., Huntington, J. L. Evaporative demand: dynamics and opportunities in drought early warning, monitoring, and vulnerability assessment. In: Proceedings of the Sixth Interagency Conference on Research in the Watersheds, DRI, Shepherdstown, USA, 211, 2019.

INETER, ANA, UNI, and GIZ-PROATAS: Cuencas Hidrográficas de Nicaragua bajo la metodología Pfafstetter, 2014. https://cira.unan.edu.ni/wp-content/uploads/2016/07/Album-Cuencas-Nic-Revisado_ANA.pdf

Jabro, J. D., Evans, R. G., Kim, Y., Iversen, W. M. Estimating in situ soil–water retention and field water capacity in two contrasting soil textures, Irrig. Sci., 27, 223–229, https://doi.org/10.1007/s00271-008-0137-9, 2009.

Kibler, C. L., Trugman, A. T., Roberts, D. A., Still, C. J., Scott, R. L., Caylor, K. K., Stella, J. C., Singer, M. B. Evapotranspiration regulates leaf temperature and respiration in dryland vegetation, Agric. For. Meteorol., 339, 109560, https://doi.org/10.1016/j.agrformet.2023.109560, 2023.

Kogan, F. N. Application of vegetation index and brightness temperature for drought detection, Adv. Space Res., 15, 91–100, https://doi.org/10.1016/0273-1177(95)00079-T, 1995.

Kozlowski, T. T.: Water deficits and plant growth, Academic Press, New York, 1968.

Leasor, Z. T., Quiring, S. M., Svoboda, M. D. Utilizing objective drought severity thresholds to improve drought monitoring, J. Appl. Meteorol. Climatol., 59, 1455–1470, https://doi.org/10.1175/JAMC-D-19-0217.1, 2020.

Li, X., Piao, S., Huntingford, C., Peñuelas, J., Yang, H., Xu, H., Chen, A., Friedlingstein, P., Keenan, T. F., Sitch, S., Wang, X., Zscheischler, J., Mahecha, M. D. Global variations in critical drought thresholds that impact vegetation, Natl. Sci. Rev., 10, nwad049, https://doi.org/10.1093/nsr/nwad049, 2023.

Lopez, A., Haines, S. Exploring the usability of probabilistic weather forecasts for water resources decision-making in the United Kingdom, Weather Clim. Soc., 9, 701–715, https://doi.org/10.1175/WCAS-D-16-0072.1, 2017.

Lovino, M. A., Pierrestegui, M. J., Müller, O. V., Müller, G. V., Berbery, E. H. The prevalent life cycle of agricultural flash droughts, npj Clim. Atmos. Sci., 7, 1–11, https://doi.org/10.1038/s41612-024-00618-0, 2024.

Ma, W., Zhang, X., Zhen, Q., Zhang, Y. Effect of soil texture on water infiltration in semiarid reclaimed land, Water Qual. Res. J., 51, 33–41, https://doi.org/10.2166/wqrjc.2015.025, 2015.

Marzban, C. The ROC curve and the area under it as performance measures, Weather Forecast., 19, 1106–1114, https://doi.org/10.1175/825.1, 2004.

McEwen, L., Bryan, K., Black, A., Blake, J., Afzal, M. Science-narrative explorations of drought thresholds in the maritime Eden catchment, Scotland: implications for local drought

https://doi.org/10.5194/egusphere-2026-1010
Preprint. Discussion started: 10 March 2026

risk management, Front. Environ. Sci., 9, 589980, https://doi.org/10.3389/fenvs.2021.589980, 2021.

Nan, Y., Chai, K. M., Lee, W. S., Chieu, H. L. Optimizing F-measure: a tale of two approaches, Proc. 29th Int. Conf. Mach. Learn., arXiv:1206.4625, https://doi.org/10.48550/arXiv.1206.4625, 2012.

Nguyen, N. M., Choi, M. Delving into flash droughts in Vietnam during last two decades using the standardized evaporative stress ratio, J. Hydrol., 634, 130669, https://doi.org/10.1016/j.jhydrol.2024.130669, 2024.

Noguera, I., Vicente-Serrano, S. M., Domínguez-Castro, F. The rise of atmospheric evaporative demand is increasing flash droughts in Spain during the warm season, Geophys. Res. Lett., 49, e2021GL097703, https://doi.org/10.1029/2021GL097703, 2022.

Or, D., Lehmann, P. Surface evaporative capacitance: how soil type and rainfall characteristics affect global-scale surface evaporation, Water Resour. Res., 55, 519–539, https://doi.org/10.1029/2018WR024050, 2019.

Otkin, J. A., Svoboda, M., Hunt, E. D., Ford, T. W., Anderson, M. C., Hain, C., and Basara, J. B.: Flash Droughts: A Review and Assessment of the Challenges Imposed by Rapid-Onset Droughts in the United States, Bulletin of the American Meteorological Society, 99, 911–919, https://doi.org/10.1175/BAMS-D-17-0149.1, 2018.

Otkin, J. A., Svoboda, M., Hunt, E. D., Ford, T. W., Anderson, M. C., Hain, C., Basara, J. B. Flash droughts: a review and assessment of the challenges imposed by rapid-onset droughts in the United States, Bull. Am. Meteorol. Soc., 99, 911–919, https://doi.org/10.1175/BAMS-D-21-0288.1, 2022.

Padiyedath Gopalan, S., Kawamura, A., Amaguchi, H., Takasaki, T., Azhikodan, G. A bootstrap approach for the parameter uncertainty of an urban-specific rainfall–runoff model, J. Hydrol., 579, 124195, https://doi.org/10.1016/j.jhydrol.2019.124195, 2019.

Portele, T. C., Lorenz, C., Dibrani, B., Laux, P., Bliefernicht, J., Kunstmann, H. Seasonal forecasts offer economic benefit for hydrological decision making in semi-arid regions, Sci. Rep., 11, 10581, https://doi.org/10.1038/s41598-021-89564-y, 2021.

Quichimbo, E. A., Singer, M. B., Michaelides, K., Hobley, D. E. J., Rosolem, R., Cuthbert, M. O. DRYP 1.0: a parsimonious hydrological model of dryland partitioning of the water balance, Geosci. Model Dev., 14, 6893–6917, https://doi.org/10.5194/gmd-14-6893-2021, 2021.

Rojas, O. Agricultural extreme drought assessment at global level using the FAO-Agricultural Stress Index System (ASIS), Weather Clim. Extremes, 27, 100184, https://doi.org/10.1016/j.wace.2018.09.001, 2020.

Rojas, O., Rodriguez de España, M. V., Hernández, T. New canicula index to study its impact on agriculture in the Central American Dry Corridor and its connection with El Niño, FAO, Rome, Italy, 67 pp., https://doi.org/10.4060/cb1818es, 2020.

Salinas Marcenaro, I., Jarquin Diaz, J. R., Ortega Flores, G. J., Téllez Reyes, A. L. La evapotranspiración potencial en Nicaragua usando sensores remotos. Universidad Nacional Agraria, Managua, Nicaragua, 2023. https://repositorio.una.edu.ni/4715/1/RENP40U58.pdf,

https://doi.org/10.5194/egusphere-2026-1010
Preprint. Discussion started: 10 March 2026

890 Salmoral, G., Rey, D., Rudd, A., de Margon, P., Holman, I. A probabilistic risk assessment of
891 the national economic impacts of regulatory drought management on irrigated agriculture,
892 Earths Future, 7, 178–196, https://doi.org/10.1029/2018EF001092, 2019.

893 Sawilowsky, S. Misconceptions leading to choosing the t test over the Wilcoxon Mann-
894 Whitney test for shift in location parameter, J. Mod. Appl. Stat. Methods, 4, 598–600,
895 https://doi.org/10.22237/jmasm/1130804700, 2005.

896 Shyrokaya, A., Pappenberger, F., Pechlivanidis, I., Messori, G., Khatami, S., Mazzoleni, M.,
897 Di Baldassarre, G. Advances and gaps in the science and practice of impact-based forecasting
898 of droughts, WIREs Water, 11, e1698, https://doi.org/10.1002/wat2.1698, 2024.

899 Solh, M., van Ginkel, M. Drought preparedness and drought mitigation in the developing
900 world's drylands, Weather Clim. Extremes, 3, 62–66,
901 https://doi.org/10.1016/j.wace.2014.03.003, 2014.

902 Soltani, A., Meinke, H., de Voil, P. Assessing linear interpolation to generate daily radiation
903 and temperature data for use in crop simulations, Eur. J. Agron., 21, 133–148,
904 https://doi.org/10.1016/S1161-0301(03)00044-3, 2004.

905 Son, N.-T., Chen, C.-F., Chen, C.-R., Castellón, A., Masferrer, M.-G.-M., Recinos, L.-E.-M.
906 Satellite characterization of drought over cultivated areas in Central America, Int. J. Remote
907 Sens., 39, 8505–8526, https://doi.org/10.1080/01431161.2018.1488287, 2018.

908 Steve, R., Qiaozhen, M., Maosheng, Z., and Alvaro, M. MODIS/Aqua Net Evapotranspiration
909 Gap-Filled Yearly L4 Global 500m SIN Grid V061,
910 https://doi.org/10.5067/MODIS/MYD16A3GF.061, 2021.

911 Suliman, M., Scaini, A., Manzoni, S., Vico, G. Soil properties modulate actual
912 evapotranspiration, and precipitation impacts on crop yields in the USA, Sci. Total Environ.,
913 949, 175172, https://doi.org/10.1016/j.scitotenv.2024.175172, 2024.

914 Sun, X., Wilcox, B. P., Zou, C. B. Evapotranspiration partitioning in dryland ecosystems: a
915 global meta-analysis of in situ studies, J. Hydrol., 576, 123–136,
916 https://doi.org/10.1016/j.jhydrol.2019.06.022, 2019.

917 Svoboda, M., LeComte, D., Hayes, M., Heim, R., Gleason, K., Angel, J. J. R. J., Rippey, B.,
918 Tinker, R., Palecki, M., Stooksbury, D., Miskus, D., Stephens, D. The Drought Monitor, Bull.
919 Am. Meteorol. Soc., 83, 1181–1190, https://doi.org/10.1175/1520-
920 0477(2002)083%253C1181:TDM%253E2.3.CO;2, 2002.

921 Teleubay, Z., Quiring, S. M., Leasor, Z. Estimation of impacts-based drought thresholds for the
922 U.S. Corn Belt, Agric. For. Meteorol., 372, 110715,
923 https://doi.org/10.1016/j.agrformet.2025.110715, 2025.

924 Teluguntla, P., Thenkabail, P., Oliphant, A., Gumma, M., Aneece, I., Foley, D., McCormick,
925 R. Landsat-derived global rainfed and irrigated-cropland product, 30 m, version 001, NASA
926 EOSDIS Land Processes DAAC,
927 https://doi.org/10.5067/COMMUNITY/LGRIP/LGRIP30.001, 2023.

928 Teoh, K. K., Ibrahim, H., Bejo, S. K. Investigation on several basic interpolation methods for
929 use in remote sensing application, in 2008 IEEE Conference on Innovative Technologies in

https://doi.org/10.5194/egusphere-2026-1010
Preprint. Discussion started: 10 March 2026

930 Intelligent Systems and Industrial Applications, 60–65,
931 https://doi.org/10.1109/CITISIA.2008.4607336, 2008.

932 Torelló-Sentelles, H., Franzke, C. L. E. Drought impact links to meteorological drought
933 indicators and predictability in Spain, Hydrol. Earth Syst. Sci., 26, 1821–1844,
934 https://doi.org/10.5194/hess-26-1821-2022, 2022.

935 Tu, Z., Yang, Y. On the estimation of potential evaporation under wet and dry conditions,
936 Water Resour. Res., 58, e2021WR031486, https://doi.org/10.1029/2021WR031486, 2022.

937 Ubeda Trujillo, I., Rocha, L. Dinámica de coberturas de la tierra en la subcuenca III de la
938 cuenca sur del Lago de Managua, Nicaragua, Rev. Torreón Univ., 9, 110–128,
939 https://doi.org/10.5377/torreon.v9i25.9857, 2020.

940 Verbist, K., Maureira, H., Aroche, R. Midsummer drought atlas for Central America and the
941 Caribbean. Water Centre for Arid and Semi-arid Zones of Latin America and the Caribbean
942 (UNESCO), 46 pp., 2018.

943 Wankmüller, F. J. P., Delval, L., Lehmann, P., Baur, M. J., Cecere, A., Wolf, S., Or, D.,
944 Javaux, M., Carminati, A. Global influence of soil texture on ecosystem water limitation,
945 Nature, 635, 631–636, https://doi.org/10.1038/s41586-024-08089-2, 2024.

946 Yu, M., Zhang, J., Wei, L., Wang, G., Dong, W., Liu, X. Impact of soil textures on agricultural
947 drought evolution and field capacity estimation in humid regions, J. Hydrol., 626, 130257,
948 https://doi.org/10.1016/j.jhydrol.2023.130257, 2023.

949 Yuan, X., Wang, L., Wu, P., Ji, P., Sheffield, J., Zhang, M. Anthropogenic shift towards higher
950 risk of flash drought over China, Nat. Commun., 10, 4661, https://doi.org/10.1038/s41467-019-
951 12692-7, 2019.

952 Yuan, X., Wang, Y., Ji, P., Wu, P., Sheffield, J., Otkin, J. A. A global transition to flash
953 droughts under climate change, Science., 380, 187–191,
954 https://doi.org/10.1126/science.abn6301, 2023.

955 van der Zee Arias, A., van der Zee, J., Meyrat, A., Poveda, C., Picado, L. Estudio de
956 caracterización del Corredor Seco Centroamericano. FAO, Tegucigalpa, Honduras, 2012.
957 https://bibliotecasemiaridos.ufv.br/jspui/handle/123456789/367

958 Zhu, Y., Toth, Z., Wobus, R., Richardson, D., Mylne, K. Economic value of ensemble-based
959 weather forecasts, Bull. Am. Meteorol. Soc., 83, 73–83, https://doi.org/10.1175/1520-
960 0477(2002)083<0073:TEVOEB>2.3.CO;2, 2002.